Active and Reactive Currents Decomposition-Based Control of Angle and Magnitude of Current for a Parallel Multiinverter IPT System

Yong Li, *Student Member, IEEE*, Ruikun Mai, *Member, IEEE*, Liwen Lu, and Zhengyou He, *Senior Member, IEEE*

***Abstract*—In order to improve the power capacity of the resonant inverter that feeds the inductive power transfer (IPT) system for high-power applications, a parallel multiinverter IPT system is presented here to upgrade the power level of the IPT system. Besides, a quick and accurate active and reactive currents decomposition method without phase-locked loop is also proposed so that the active and reactive currents can be controlled independently. This method can minimize the circulating current caused by asymmetrical resonant components and different dc input voltages. Meanwhile, the track current can be regulated at its designed value with a fast response performance. Moreover, a protection device and a protection scheme are designed to disconnect the fault inverter unit, which can ensure that the whole system works continuously so as to improve the reliability and availability dramatically. Finally, a 3-kW experimental setup using a two-inverter IPT system is conducted to verify the performance of the proposed method. The overall efficiency of the improved IPT system is up to 93.5% at 2.87 kW output, and the experimental results also indicate that the proposed method improves the stability of track current control and achieves circulating current minimization.**

***Index Terms*—Active and reactive currents decomposition, circulating current, inductive power transfer (IPT), parallel multiinverter, phase-locked loop (PLL), track current control.**

I. Introduction

INDUCTIVE power transfer (IPT) systems can deliver electric power from primary power source to secondary load side through magnetic coupling without physical contact [1]–[4]. Such systems have numerous advantages, e.g., they are unaffected by ice, water, and other chemicals, and are thereby environment friendly and maintenance free. Nowadays, IPT systems have been used in various applications including wireless charging of biomedical implants [5], [6], mining applications [7], underwater power supplies [8], and electric vehicles [9]–[17].

Generally, an IPT system is composed of a power supply in the primary side, a pickup in the secondary side, and magnetic structures for inductive coupling. For IPT systems, the power supply, which is a resonant inverter, is one of the most important components in the whole system, and it generates a high-frequency current in the primary side. However, the power capacity of a single resonant inverter is limited by the constraints of power electronic devices and the economic constraints.

Recently, IPT systems have been successfully applied to public transport systems (such as electric vehicles and electric trains [18]). The secondary systems are electrically isolated and can move along a long track energized by the resonant inverter. The advantages of such systems are safety, reliability, low maintenance, and long product life span. Most of the researches conducted on IPT public transport systems have focused on circuit topologies, system efficiency, and magnetic coupling design [14]–[17]. Unfortunately, very few concerns with the high demand power suitable for multiple public transport systems and electric trains. The power supplies used for public transport systems need to be rated at hundreds of kilovoltampere or more (up to megawatt scale) due to the high power demands of the electric trains [18].

As a possible solution, high-voltage, high-current, and high-frequency semiconductor devices are used to implement the demanded high power for the high-power applications. However, such semiconductor devices are relatively expensive or not available in the commercial market. Therefore, it is desirable and significant to enhance the power capacity of the resonant inverter by using low-power and low-cost semiconductor devices.

The reported methods [21]–[25] to enhance the power capacity of the resonant inverter feeding IPT systems can be classified into two categories as far as we known:

1) multilevel resonant inverter supplies IPT systems;
2) parallel multiinverter supplies IPT systems.

Multilevel technology [21]–[23] has advantage in aspects in reducing voltage stress of semiconductor devices, and implementing high-power IPT systems by using low-cost and low-voltage semiconductor devices. However, it would be a challenge to implement such a system at high frequency and the cascaded structure of the multilevel inverter dramatically decreases the WPT system reliability.

Alternatively, parallel multiinverter can achieve high-power capacity by integrating low-power capacity resonant inverters [24]–[26]. The parallel multiinverter IPT system has the following advantages [26], [27]. First, the limitation of single resonant inverter unit can be removed in terms of cost, heating dissipation, component limitation, and short-time overload. Second, the paralleling of several resonant inverter units also brings convenience for flexible operation for maximum output power and

Manuscript received December 11, 2015; revised March 8, 2016; accepted April 2, 2016. Date of publication April 5, 2016; date of current version November 11, 2016. This work was supported by the National Natural Science Foundation of China under Grant 51507147, by the National Science Fund for Distinguished Young Scholars (51525702), and by the Independent Research Subject of the State Key Laboratory of Traction Power (2016TPL_T11). Recommended for publication by Associate Editor J. M. Rivas Davila.

The authors are with the School of Electrical Engineering, Southwest Jiaotong University, Sichuan 610031, China (e-mail: leeo1864@163.com; mairk@swjtu.edu.cn; 953390550@qq.com; hezy@swjtu.edu.cn).

Color versions of one or more of the figures in this paper are available online at http://ieeexplore.ieee.org.

Digital Object Identifier 10.1109/TPEL.2016.2550622

reducing manufacturing cost. For example, we can use two existing 50-kW IPT power supplies to achieve 100-kW IPT power supply, which is an efficient way to realize high power rather than redesign and remanufacture the power supply. Third, the system reliability is also increased with designed redundancy. Therefore, parallel multiinverter is one of the desirable methods to enhance the power capacity of the primary converter for supplying IPT systems.

A parallel connected system for induction heating based on the high-frequency *LCL* resonant inverter was described in [24]. It does not requires additional devices for connecting inverters in parallel, and the flexible power levels can be achieved by choosing the number of parallel inverters. A parallel topology, which can achieve high output power levels in a cost-effective manner for IPT systems with *LCL*-T resonant inverters, is proposed in [25], with high reliability of functioning, even that a faulty parallel unit is electronically shut down. However, both of them did not investigate the control strategy of the circulating current minimization and the track current maintenance. A novel control scheme to minimize the circulating current based on the active and reactive current decomposition concept instead of phase angle and amplitude of the current is proposed in [26]. However, the system only considered the resistive load and did not investigate and design a protection device to disconnect the defected inverter from the parallel inverter units. In addition, the active and reactive current decomposition based on the active and reactive power theory by using the phase-locked circuits or other circuits to track the output voltage frequency and phase, which increases the control system complexity.

Circulating current is a critical issue in the parallel multiinverter IPT system. Large circulating currents among the inverter units caused by the component tolerance and other forms of uncertainties increase the power loss and overcurrent/overload in the inverter units [26], [27]. Therefore, the circulating currents should be minimized by an effective current sharing control method. In order to simplify the pickup control, it is necessary to regulate the track current at its designed value as the received voltage by a pickup is directly proportional to the track current [19]. Meanwhile, when multiple electric vehicles and electric trains are powered simultaneously, which also prefers a constant current in the track [20].In addition, a fault in one of the parallel units may force the whole system to shut down without sophisticated protection procedure. To achieve high reliability, it is desirable to design a protection device to disconnect the fault inverter from the parallel inverter units, and the rest of the unit can continue to perform its functionality in order to dramatically improve the reliability and availability.

This paper attempts to realize constant control of the track current and minimization of the circulating current for the high power transfer of IPT systems by connecting low-power capacity resonant inverters in parallel. A novel control method based on the active and reactive currents decomposition without phase-locked loop (PLL) is proposed in this paper by defining virtual active and reactive powers. The circulating current can be minimized by the proposed control method. Furthermore, the track current can be regulated at its designed value according to the required power with a quick response within 10 ms.

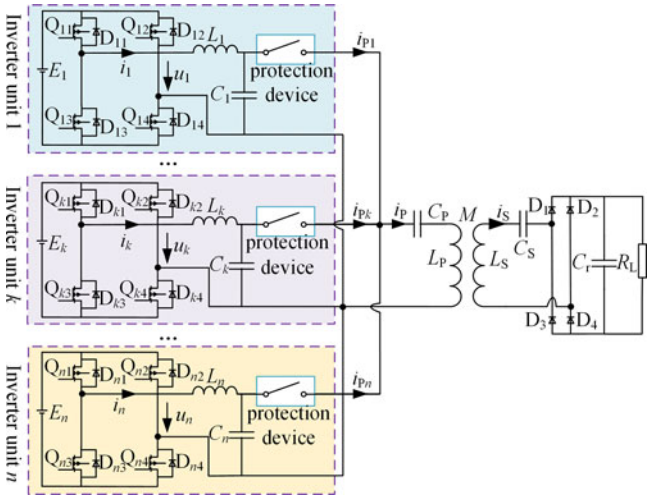

Fig. 1. *LCL*-S tuned IPT system based on multiinverter.

A protection device and a protection scheme are designed to disconnect the fault inverter unit, which can ensure the whole system to work continuously so as to improve the reliability and availability dramatically.

II. Basic Principle of Parallel Multiinverter Supplying IPT Systems

Various compensation topologies have been proposed and implemented to tune the primary track and secondary coil at the resonant frequency to achieve high efficiency for the whole IPT system. An *LCL* compensation is formed by adding an *LC* compensation network between the inverter and the primary track. There are some advantages for the *LCL* compensation when the network tuned at the resonant frequency as following:

1) the inverter only supplies the active power required by the load without any reactive power;
2) the current in the primary track is independent of the load;
3) it does not require additional devices for connecting inverters in parallel.

Therefore, multiple parallel *LCL*-based resonant inverters supplying the primary track are employed in this paper, and a compensating capacitor is connected in series with the secondary coil to tune the pickup circuit. The schematic diagram of the proposed parallel multiinverter *LCL*-Series (*LCL*-S) tuned IPT system is illustrated in Fig. 1. Nowadays, many topologies achieving bidirectional power transfer capability have been proposed and investigated such as [28]–[30], which are excluded from consideration in this paper.

Each inverter unit consists of a voltage-fed high-frequency inverter, an *LC* compensation network, and a protection device which will be illustrated in Section III-B. The voltage-fed high-frequency inverters are separately powered by isolated dc supplies, which can be different energy sources, e.g., the dc bus (rectified by utility power), batteries, and/or photovoltaic (PV) shown in Fig. 2.

The operating angular frequency of the inverters is ω.The second inductor $L_{\rm eq}$ of the *LCL* resonant tank is formed by the primary coil L_P and C_P. $L_{\rm eq}$ can be configured by the C_P. So

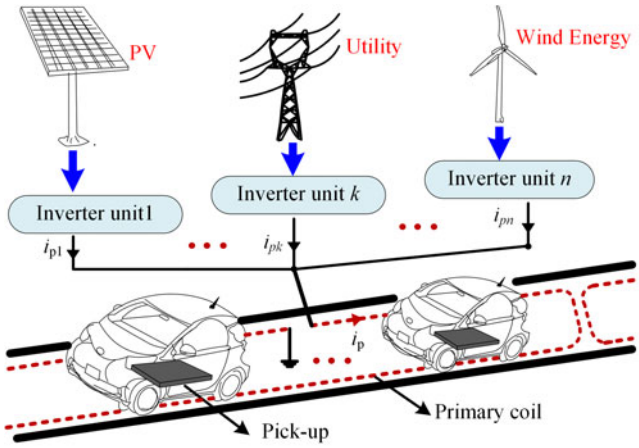

Fig. 2. Potential application of the proposed IPT system.

$L_{\rm eq}$ can be expressed as $L_{\rm eq} = L_P - \frac{1}{\omega^2 C_P}$, correspondingly. The synthesized current i_P flowing through the primary coil L_P establishes magnetic coupling with the pickup. The secondary circuit consists of the pick-up coil L_S, the compensation capacitor C_S, the full-bridge rectifier, and the load R_L.

The synthesized current i_P can be expressed as

$$i_P = \sum_{k=1}^{n} i_{\rm Pk} \tag{1}$$

Owe to the parallel topology, the magnetic flied established by the track current can be enhanced.

A. Parameter Design and Analyze of the Parallel IPT System

According to Hu [19], the equivalent load R_0 of the rectified tank connected to a resistive load R_L can be expressed as

$$R_0 = \frac{8R_L}{\pi^2} \tag{2}$$

At steady state, assuming the pickup is completely tuned $\left(\omega = \frac{1}{\sqrt{L_S C_S}}\right)$, the reflected impedance of the secondary circuit becomes purely resistive load [19], which can be derived as

$$R_{\rm eq} = \frac{\omega^2 M^2}{R_0} = \frac{\pi^2 \omega^2 M^2}{8R_L} \tag{3}$$

According to Schonknecht and De Doncker [24] and Hao *et al.* [25], for tuning purposes, L_{k1} and C_{k1} should meet the following equation:

$$\omega = \frac{1}{\sqrt{L_k C_k}}, \quad (k = 1, 2, 3, \ldots, n) \tag{4}$$

The output voltage of the inverter is controlled by the phase-shifted pulse width modulation. In order to achieve zero-voltage switching (ZVS) turn-on for all the parallel voltage-fed inverters, $L_{\rm eq}$ should be configured to make the impedances of the inverters to be inductive [31], [32], so as to reduce the loss of the voltage-fed inverters and suppress the electromagnetic interference by decreasing the peak currents of the switches. Under this condition, the output current of the voltage-fed inverter lags behind the output voltage [31]. The relevant voltage and current

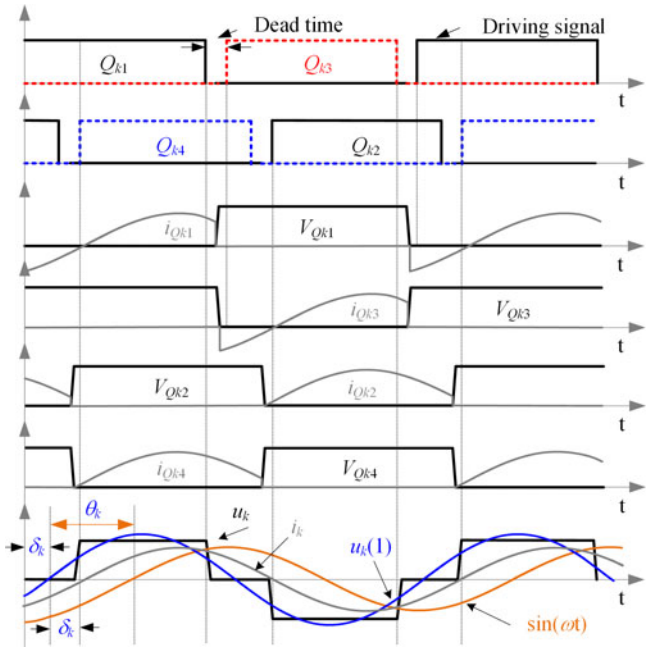

Fig. 3. Relevant voltage and current operating waveforms.

waveforms are shown in Fig. 3, and all the inverters operate at inductive mode. V_{Qk1}, V_{Qk2}, V_{Qk3}, and V_{Qk4} are the voltages across power MOSFETs and i_{Qk1}, i_{Qk2}, i_{Qk3}, and i_{Qk4} are the currents through power MOSFETs. The current and voltage waveforms of the MOSFETs in the same half-bridge are identical but with a certain delay.

During the turn-on period of all the MOSFETs, the driving signals have a certain lag with respect to the voltages across the corresponding MOSFETs. It is evident that all the MOSFETs can be turned ON with zero voltage, so all the MOSFETs can achieve ZVS turn-on operation.

The fundamental output voltage of the *k*th inverter can be expressed as

$$u_k(1) = \frac{4E_k}{\pi} \cos\delta_k \sin(\omega t + \theta_k) \tag{5}$$

where E_k is the dc-link voltage, δ_k is half of the phase-shift angle between the two legs of the inverter, and θ_k is the angle between the output voltage and the reference signal $\sin(\omega t)$. By regulating δ_k and θ_k, both the amplitude and phase angle of the output voltage can be controlled instead of adding an buck converter for controlling the dc-link voltage.

The fundamental voltage phasor of the *k*th inverter can be expressed as

$$\dot{U}_k = \frac{4E_k}{\pi} \cos\delta_k \cos\theta_k + j\frac{4E_k}{\pi} \cos\delta_k \sin\theta_k \tag{6}$$

B. Influencing Factors of Circulating Current

In order to analyze the circulating currents among the inverter units, two-inverter-based case is studied here without loss of generality. The equivalent circuit of a two-inverter parallel system is demonstrated in Fig. 4.

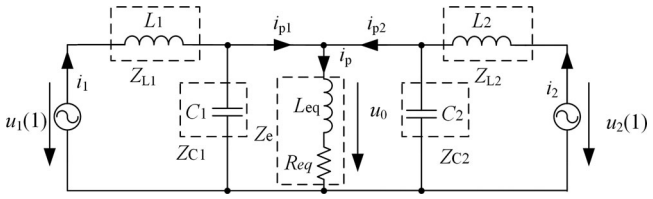

Fig. 4. Equivalent circuit of the IPT system with parallel two inverter.

According to Kirchhoff's current law, we can get

$$\frac{\dot{U}_1-\dot{U}_0}{Z_{L1}}-\frac{\dot{U}_0}{Z_{C1}}+\frac{\dot{U}_2-\dot{U}_0}{Z_{L2}}-\frac{\dot{U}_0}{Z_{C2}}=\frac{\dot{U}_0}{Z_e} \tag{7}$$

where $Z_{L1}=j\omega L_1, Z_{L2}=j\omega L_2, Z_{C1}=\frac{1}{j\omega C_1}, Z_{C2}=\frac{1}{j\omega C_2}$, and $Z_e=j\omega L_{\rm eq}+R_{\rm eq}$.

Combining (6) and (7), the currents of each inverter unit are given by equation (8)–(9) as shown at the bottom of the page.

According to Ye *et al.* [26], the circulating current between the first and the second inverter units can be expressed by

$$\dot{I}_c=\frac{\dot{I}_{P1}-\dot{I}_{P2}}{2} \tag{10}$$

Substituting (6), (8), and (9) into (10), the fundamental circulating current phasor can be obtained by equation (11) as shown at the bottom of the page.

where $A=Z_{C1}Z_{C2}$, $B=Z_{L1}Z_{L2}$, $C=Z_{C1}Z_{L2}$, and $D=Z_{C2}Z_{L1}$.

Assuming $Z_{L1}=-Z_{C1},\ Z_{C1}=Z_{C2},\ Z_{L1}=k_zZ_{L2},\ k_z$ is the tolerances coefficient which shows the relationship of Z_{L1} and Z_{L2} due to the inevitable tolerances of commercial inductors. The output voltages of each inverter unit may not be identical (with different amplitude and phase) due to the component tolerance, gate driver delay, and the input dc voltage fluctuation. Therefore, the output voltage of each inverter follows the relationship of $\dot{U}_1=(k_{u1}+jk_{u2})\dot{U}_2$.

For simplicity, assuming that there are two cases listed below.

For case I, all the resonant components are identical but with different output voltage ($k_z=1, k_{u1}+jk_{u2}\neq 1$), we can get

$$\dot{I}_c=\frac{\dot{U}_2Z_{C2}(k_{u1}+jk_{u2}-1)}{2}\neq 0 \tag{12}$$

It indicates that the circulating current exists because of the different output voltage even with identical resonant inductors.

TABLE I
DESIGN SPECIFICATIONS AND CIRCUIT PARAMETERS OF IPT PROTOTYPE

Parameters	Value
Inverter frequency *f*/kHz	20
resonant inductance L_f /μH	130.99
resonant capacitance C_f /nF	498.75
Inductance of the primary coil L_P /μH	608.26
The resonant inductance of H_1 L_1 /μH	136
The resonant inductance of H_2 L_2 /μH	123.5
The resonant capacitance of H_1 C_1 /nF	501.6
The resonant capacitance of H_2 C_2 /nF	500.5
Compensation capacitance of primary circuit C_P /nF	112.6
Mutual inductance of the primary and secondary coils *M*/μH	129.1
Inductance of the secondary coil L_S /μH	507.34
Compensation capacitance of secondary circuit C_S /nF	124.8
Equivalent resistance of the load R_L /Ω	12
MOSFET: IRF640N	

For case II, all the output voltages are identical but with possible different resonant components ($k_{u1}+jk_{u2}=1$, $k_z\neq 1$), we can get

$$\dot{I}_c=\frac{\dot{U}_2Z_{C2}(Z_{C2}+2Z_e)(k_z-1)}{2Z_{C2}^2Z_e(k_z+1)+2(Z_{C2}+2Z_e)}\neq 0 \tag{13}$$

As discussed above, the circulating current can exist among the inverters because of the different output voltages and asymmetrical resonant components.

Moreover, it is desirable to investigate the sensitivity of each component to the circulating current. The parameters of the IPT system for the circulating current analysis is shown in Table I. For simplicity, the sensitivity of the resonant inductors to the circulating current is investigated under the condition that all the output voltages are identical ($k_{u1}+jk_{u2}=1$), and the tolerance coefficient of the inductors follows $0.8\leq k_z\leq 1.2$ (for a practical inverter, the tolerance of the commercially available resonant components is above 10%). Therefore, the normalized circulating current caused by asymmetrical inductors is shown in Fig. 5.

Similarly, the normalized circulating current caused by asymmetrical voltages ($0.8\leq k_{u1}\leq 1.2$ and $-0.5\leq k_{u2}\leq 0.5$) while with identical inductors ($k_z=1$) is shown in Fig. 6.

Under the ideal condition (all the inverter units are identical), there is no circulating current in the paralleled resonant inverters. It is obvious that the circulating current increases with the resonant components tolerance and the difference between

$$\dot{I}_{P1}=\frac{\dot{U}_1Z_{C1}(Z_{C2}Z_e+Z_{C2}Z_{L2}+Z_{L2}Z_e)-\dot{U}_2Z_{C2}Z_e(Z_{C1}+Z_{L1})}{Z_{C1}Z_{C2}(Z_{L1}Z_e+Z_{L1}Z_{L2}+Z_{L2}Z_e)+Z_{L1}Z_{L2}Z_e(Z_{C2}+Z_{C1})} \tag{8}$$

$$\dot{I}_{P2}=\frac{\dot{U}_2Z_{C2}(Z_{C1}Z_e+Z_{C1}Z_{L1}+Z_{L1}Z_e)-\dot{U}_1Z_{C1}Z_e(Z_{C2}+Z_{L2})}{Z_{C1}Z_{C2}(Z_{L1}Z_e+Z_{L1}Z_{L2}+Z_{L2}Z_e)+Z_{L1}Z_{L2}Z_e(Z_{C2}+Z_{C1})} \tag{9}$$

$$\dot{I}_c=\frac{2Z_e\left(C\dot{U}_1-D\dot{U}_2\right)+A\left(\dot{U}_1Z_{L2}-\dot{U}_2Z_{L1}\right)+2AZ_e\left(\dot{U}_1-\dot{U}_2\right)}{2\left[AB+AZ_e\left(Z_{L1}+Z_{L2}\right)+BZ_e\left(Z_{C1}+Z_{C2}\right)\right]} \tag{11}$$

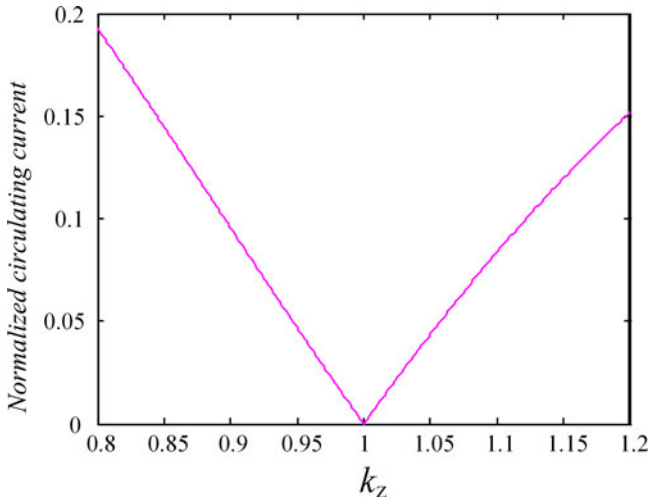

Fig. 5. Normalized circulating current versus resonant inductors' tolerance.

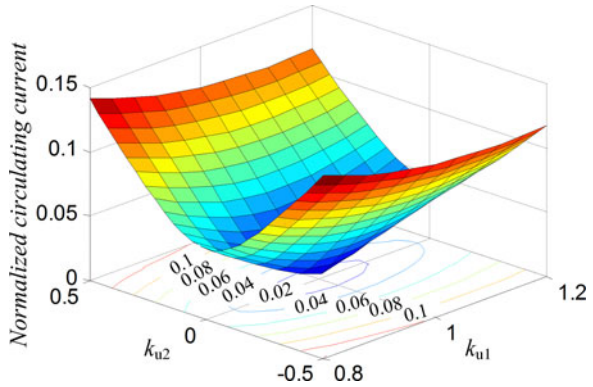

Fig. 6. Normalized circulating current versus voltages' tolerance.

the voltages. Furthermore, it is noticed that in a practical multiinverter IPT system, the circulating current can be combined results of circuit asymmetry and difference in the input voltages to the inverter units. Therefore, it is important and necessary to minimize the circulating current.

III. Current Sharing Control in Multiinverter IPT Systems

In the multiinverter-based IPT system, the decomposed active and reactive currents can be represented by a linear function instead of detecting the current amplitude and phase angle. However, the conventional approach of active and reactive currents decomposing [26], [27] needs PLL to track the phase of the voltage for calculating the active and reactive powers.

The PLL usually needs phase detection circuits to detect the phases of the signals. However, the phase detection circuit is not applicable under a small-current condition, especially with heavy noise. Moreover, it is not easy to tune the resonant circuit at the resonant frequency in practical IPT systems, which results in the track current being distortion so that the zero crossing is not the actual zero phase of the fundamental current. An improper PLL design may cause the active and reactive currents detection error which affects the system's control performance. Therefore, it is desirable to investigate an approach to decompose the active and reactive currents without PLL.

Virtual active and reactive current decomposition method without PLL is proposed here to overcome the drawbacks aforementioned. In order to let the inverter unit currents be in phase, the track current is adopted as the reference current for the inverters current to follow. Then, virtual active and reactive powers between the track current i_P and inverter unit current $i_{\rm Pk}$ are defined, but they are not the circuits or physical reaction and action in the real system. The virtual reactive power is only the reflection of the phase difference between the inverter unit current and the reference current. The virtual active power is the reflection of the inverter current that flows into the track current. Moreover, the virtual active and reactive powers can be calculated without PLL, then the active and reactive currents can be derived.

A. Active and Reactive Current Decomposition Without PLL

The synthesized current i_P, flowing through the primary track (coil) L_P, is feasible to be assumed as a pure sinusoidal signal due to the resonant network, and can be set as the reference signal

$$i_P = I_m \sin(\omega t) \tag{14}$$

where I_m is the amplitude of the current i_P.

The output current of the *k*th inverter unit can be expressed as

$$i_{\rm Pk} = I_{\rm mk} \sin(\omega t + \phi_k) = i^{\rm ak} \sin(\omega t) + i^{\rm rk} \cos(\omega t) \tag{15}$$

where $i^{\rm ak}\sin(\omega t)$ and $i^{rk}\cos(\omega t)$ are defined as the active and reactive currents against the reference signal. $I^{\rm ak}$ and $I^{\rm rk}$ are the amplitudes of the active and reactive currents, respectively, which can be expressed as

$$\begin{cases} I^{\rm ak} = I_{\rm mk} \cos(\phi_k) \\ I^{\rm rk} = I_{\rm mk} \sin(\phi_k) \end{cases} \tag{16}$$

The virtual active and reactive powers of the *k*th inverter unit current $i_{\rm Pk}$ against the track current i_P can be defined as

$$\begin{cases} P_k = \frac{I_m I_{\rm mk} \cos(\phi_k)}{2} \\ Q_k = -\frac{I_m I_{\rm mk} \sin(\phi_k)}{2} \end{cases} \tag{17}$$

Two orthogonal signals generated by the controller with the same frequency of ω and random phase angle $\phi_{\rm ref}$ can be expressed as

$$\begin{cases} \sin_C = \sin(\omega t + \phi_{\rm ref}) \\ \cos_C = \cos(\omega t + \phi_{\rm ref}) \end{cases} \tag{18}$$

The productions of (18) by the kth inverter unit current i_{Pk} and the track current i_P, respectively, can be expressed as

$$\begin{cases} i^s_{\mathrm{Pk}} = I_{\mathrm{mk}} \sin(\omega t + \phi_k) \cdot \sin_C \\ = \frac{-I_{\mathrm{mk}}[\cos(2\omega t + \phi_k + \phi_{\mathrm{ref}}) - \cos(\phi_k - \phi_{\mathrm{ref}})]}{2} \\ i^c_{\mathrm{Pk}} = I_{\mathrm{mk}} \sin(\omega t + \phi_k) \cdot \cos_C \\ = \frac{I_{\mathrm{mk}}[\sin(2\omega t + \phi_k + \phi_{\mathrm{ref}}) + \sin(\phi_k - \phi_{\mathrm{ref}})]}{2} \\ i^s_P = I_m \sin(\omega t) \cdot \sin_C \\ = \frac{-I_m[\cos(2\omega t + \phi_{\mathrm{ref}}) - \cos\phi_{\mathrm{ref}}]}{2} \\ i^c_P = I_m \sin(\omega t) \cdot \cos_C \\ = \frac{I_m[\sin(2\omega t + \phi_{\mathrm{ref}}) - \sin\phi_{\mathrm{ref}}]}{2} \end{cases} \tag{19}$$

Obviously, i^s_{Pk}, i^c_{Pk}, i^s_P, and i^c_P are composed of dc component and an second-order harmonic component. By applying an appropriate low-pass filter (LPF), the second-order harmonic component can be filtered out. Then, we can get the dc component

$$\begin{cases} i_{ak} = \frac{I_{\mathrm{mk}} \cos(\phi_k - \phi_{\mathrm{ref}})}{2} \\ i_{rk} = \frac{I_{\mathrm{mk}} \sin(\phi_k - \phi_{\mathrm{ref}})}{2} \\ i_a = \frac{I_m \cos\phi_{\mathrm{ref}}}{2} \\ i_r = \frac{-I_m \sin\phi_{\mathrm{ref}}}{2} \end{cases} \tag{20}$$

According to (20), the amplitudes of the track current and the inverter unit current can be expressed as

$$\begin{cases} I_m = 2\sqrt{i_a^2 + i_r^2} \\ I_{\mathrm{mk}} = 2\sqrt{i_{ak}^2 + i_{rk}^2} \end{cases} \tag{21}$$

Substituting (20) and (21) into (17), the virtual active and reactive powers can be rewritten as

$$\begin{cases} P_k = \frac{I_m I_{\mathrm{mk}}[\cos(\phi_k - \phi_{\mathrm{ref}})\cos\phi_{\mathrm{ref}} - \sin(\phi_k - \phi_{\mathrm{ref}})\sin\phi_{\mathrm{ref}}]}{2} \\ \quad = 2(i_a i_{ak} + i_r i_{rk}) \\ Q_k = \frac{-I_m I_{\mathrm{mk}}[\sin\phi_{\mathrm{ref}}\cos(\phi_k - \phi_{\mathrm{ref}}) + \cos\phi_{\mathrm{ref}}\sin(\phi_k - \phi_{\mathrm{ref}})]}{2} \\ \quad = 2(i_r i_{ak} - i_a i_{rk}) \end{cases} \tag{22}$$

Substituting (17), (21), and (22) into (16), the amplitudes of the active and reactive current components can be derived as

$$\begin{cases} I^{\mathrm{ak}} = \frac{2P_k}{I_m} = \frac{2(i_a i_{ak} + i_r i_{rk})}{\sqrt{i_a^2 + i_r^2}} \\ I^{\mathrm{rk}} = -\frac{2Q_k}{I_m} = \frac{2(i_a i_{rk} - i_r i_{ak})}{\sqrt{i_a^2 + i_r^2}} \end{cases} \tag{23}$$

Therefore, the virtual active and reactive currents against the track current can be calculated without PLL. The block diagram of the proposed active and reactive current decomposition named "virtual current decomposition" is provided in Fig. 7.

As shown in Fig. 8(a), the circulating current between the kth and $(k+1)$th inverter units can be decomposed into the active current component and the reactive current component against the reference current (track current) fixed to the real axis. To minimize the circulating current, both the active and reactive circulating current components should be controlled to be zero. As shown in Fig. 8(b), in other words, to keep the average of the active current components of all the inverter units to be the same, and to keep the reactive current components of all the inverter units to be zero.Therefore, the references active current $I^{\mathrm{ak}*}$ and reactive current $I^{\mathrm{rk}*}$ are explained as

$$\begin{cases} I^{\mathrm{ak}*} = \frac{1}{n}\sum_{j=1}^{n} I^{aj} = \frac{1}{n} I_m \\ I^{\mathrm{rk}*} = 0 \end{cases} \tag{24}$$

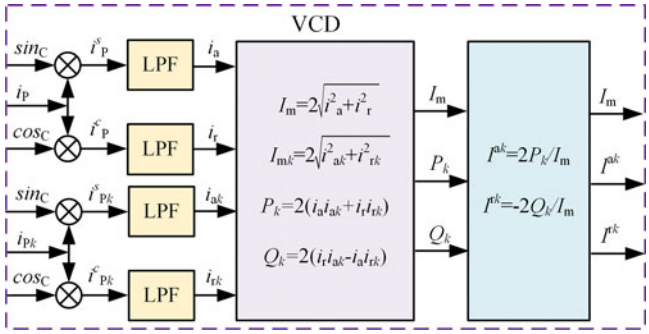

Fig. 7. Block diagram of the proposed active and reactive currents decomposition method.

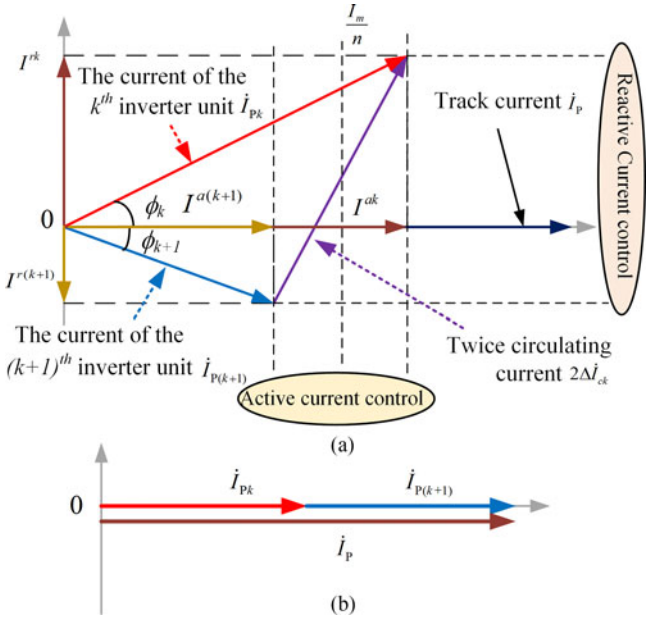

Fig. 8. Phasor diagram. (a) Active and reactive currents control, and the (b) expected control result of the inverter units' currents.

B. Protection Device and Scheme

The schematic of the protection device connected in series in the inverter units is depicted in Fig. 9. L_{fk} and C_{fk} are formed as a resonant tank to block dc offset currents among the inverter units and filter the harmonic components of the inverter unit current. As a result, the resonant tank acts as a short circuit in terms of the fundamental current. The resonant tank is made of inductor and capacitor with low equivalent series resistance (ESR). Therefore, the power loss of the resonant tank can be neglected.

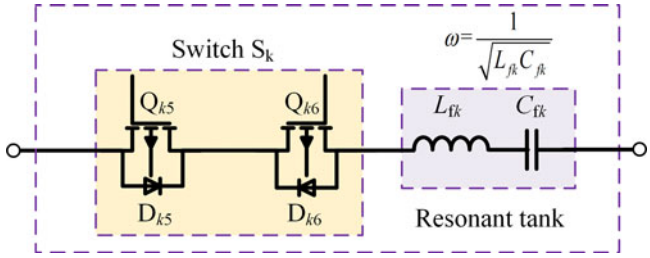

Fig. 9. Schematic of the protection device.

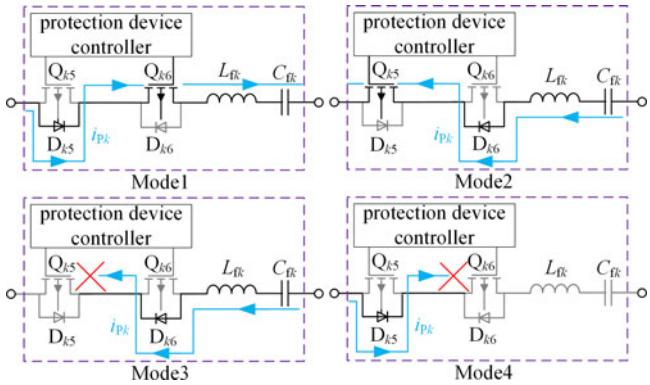

Fig. 10. Modes of the protection device.

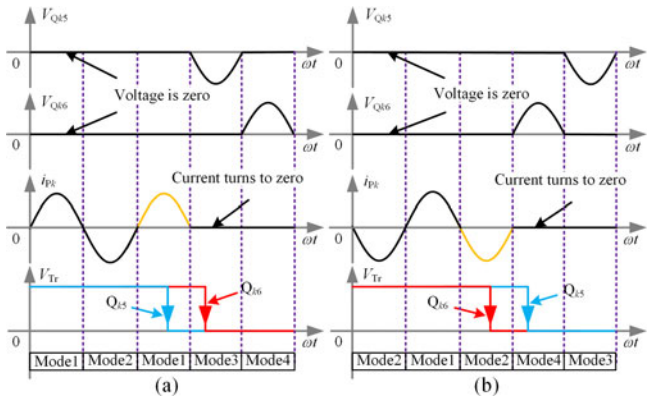

Fig. 11. Relevant voltage and current operating waveforms of the protection device.

Under normally operating condition, the driving signals of Q_{k5} and Q_{k6} are high-level voltages. One switching cycle operation is divided into two submodes: mode 1 and mode 2, as shown in Fig. 10. The voltages through Q_{k5} and Q_{k6} are zero ignoring the voltage drop of D_{k5} and D_{k6}, indicating the protection device is turned ON and the power loss of the protection device is negligible. As a result, the protection device acts as a short circuit, and the inverter unit current i_{Pk} can flow through the protection device bidirectionally. Moreover, the relevant voltage and current operating waveforms of the protection device are depicted in Fig. 11.

If the *k*th inverter unit occurs a fault, the protection device is supposed to operate to disconnect the fault unit. If the direction of i_{Pk} is forward as shown in mode1 in Fig. 11(a), where the

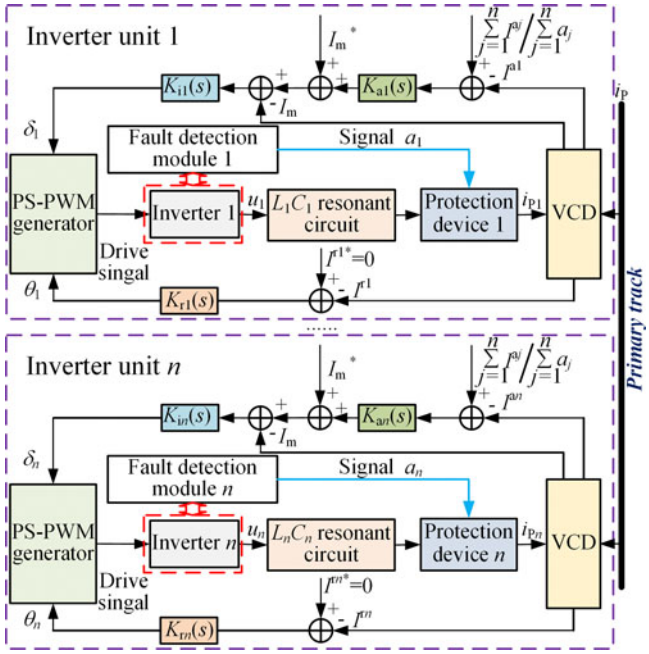

Fig. 12. Control diagram of the IPT system based on multiple inverters.

driving signal of Q_{k5} turns off. Then, Q_{k5} will shut down with ZVS since the voltage across Q_{k5} is zero. When i_{Pk} reverses, Q_{k5} can be totally shut down, and i_{Pk} should be zero as shown in mode3. The driving signal of Q_{k6} turns to be zero, and Q_{k6} can be shut down with zero current switching (ZCS) condition. Therefore, the fault inverter unit can be disconnected from the IPT system based on multiple inverters.

As shown in Fig. 11(b), the same soft switching could be achieved when the fault occurs at the i_{Pk} is negative as shown in mode 2 similarly to the case discussed above.

Therefore, the fault inverter unit can be disconnected from the multiinverter IPT system quickly with ZVS and ZCS operation. It dramatically increases the reliability of the IPT system.

C. Control Diagram for the Proposed IPT System

The active and reactive currents decomposition method-based control strategy for parallel multiinverter IPT system is shown in Fig. 12. The circulating current can be minimized by controlling the amplitude and phase of the output voltage of each inverter unit [26].

This control strategy is composed of two control feedback loops, the active and reactive currents control loops. *Kr*(*s*), *Ka*(*s*), and *Ki*(*s*) are the reactive current minimization controller, the active current sharing controller, and the primary track current feedback controller, respectively. All the controllers mentioned above are in form of proportional-integral (PI) or proportional (*P*) controllers. Each inverter is with a dedicated fault detection module, which will send signal $a = 0$ to the protection device in order to disconnect the fault unit from the whole system when a fault occurs. If the inverter unit is normally operating, $a = 1$ is sent. Then, the references active current component is changed to be $\sum_j^n I^{\mathrm{aj}} / \sum_j^n a_j$, and the reference current

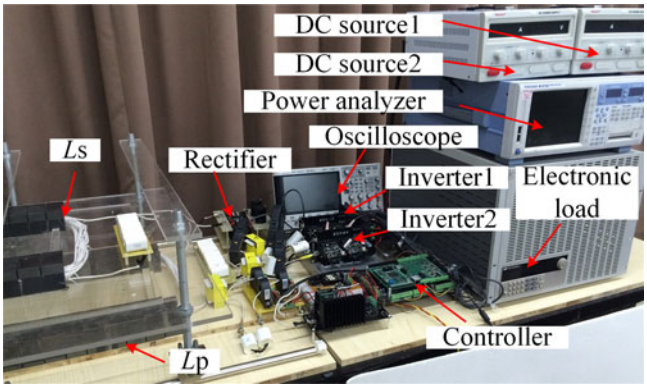

Fig. 13. Exterior appearance of the proposed IPT prototype.

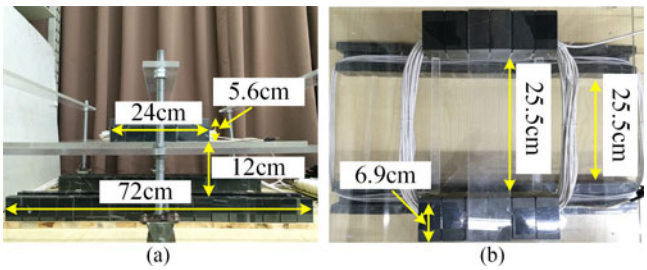

Fig. 14. Primary and the secondary coils wound with Litz wire. (a) Lateral view of the coils, and (b) top view of the coils.

component is still zero, which can maintain the whole system working continually. Thus, the reliability and availability of the IPT system can be dramatically improved.

IV. Experimental Results

A. Prototype System

To validate the proposed control method, an experimental IPT prototype based on a multiple inverter system consisting of two resonant inverter units has been constructed in the laboratory settings. The practical setup is shown in Fig. 13. A TMS320F28335 digital signal processing unit was used as the controller. CONCEPT-2SC0108T2A0-17 is adopted as the power MOSFET driver to fulfill the requirement of high switching frequency in the experiment. Moreover, it has a function of fault detection. The rectifier bridge uses fast recovery diode DSEI2x61-02A. The primary track and the pick-up coil are wound around U-type ferrite cores with Litz wires (with low ESR). The pick-up coil is deliberately designed shorter than the primary track so that it can dynamically move over the primary track freely. The coils sizes are shown in Fig. 14. The air gap between the primary track and the pick-up coil is set to be 12 cm, which may satisfy the demand of electric vehicles. The mutual and coil inductances are measured with Agilent E4980A LCR meter.

The design specifications ofthe experimental setup are listed in Table I. In the experimental evaluation, it is assumed that the H-bridge inverters have the same power rating. The

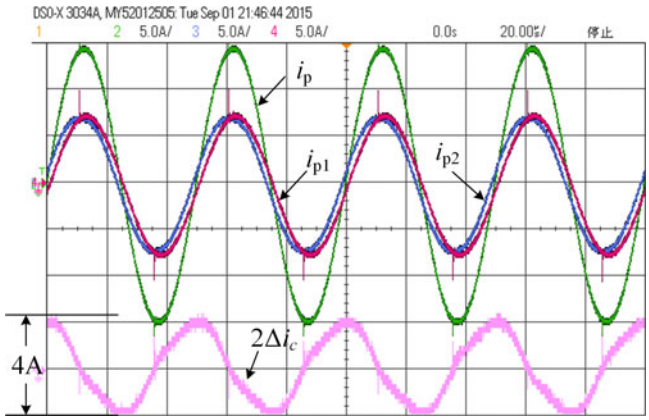

Fig. 15. Current waveforms without current sharing control under asymmetrical inductance parameters condition.

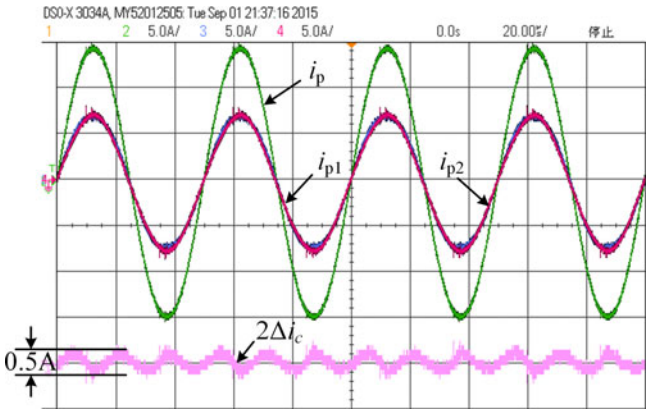

Fig. 16. Current waveforms with current sharing control under asymmetrical inductance parameters condition.

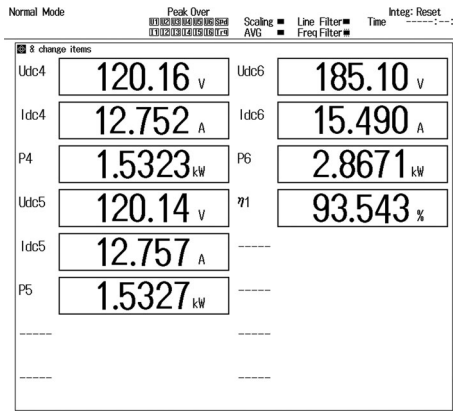

Fig. 17. Capture of power from power analyzer at 2.87 kW output with current sharing control under asymmetrical inductance parameters condition.

second-order Butterworth filter with the cut off frequency of 100 Hz has been used as the LPF.

B. Experimental Results

Variation in resonant components and/or dc source voltages can cause circulating current among the inverter units, which are illustrated as following.

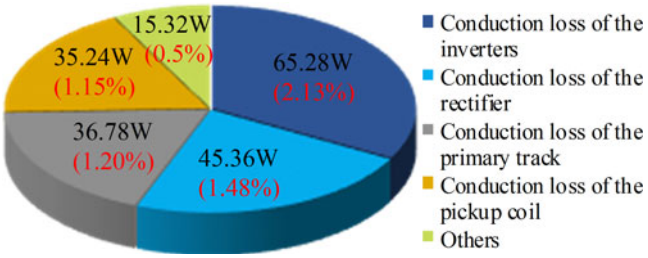

Fig. 18. Measured power loss distribution at 2.87 kW output.

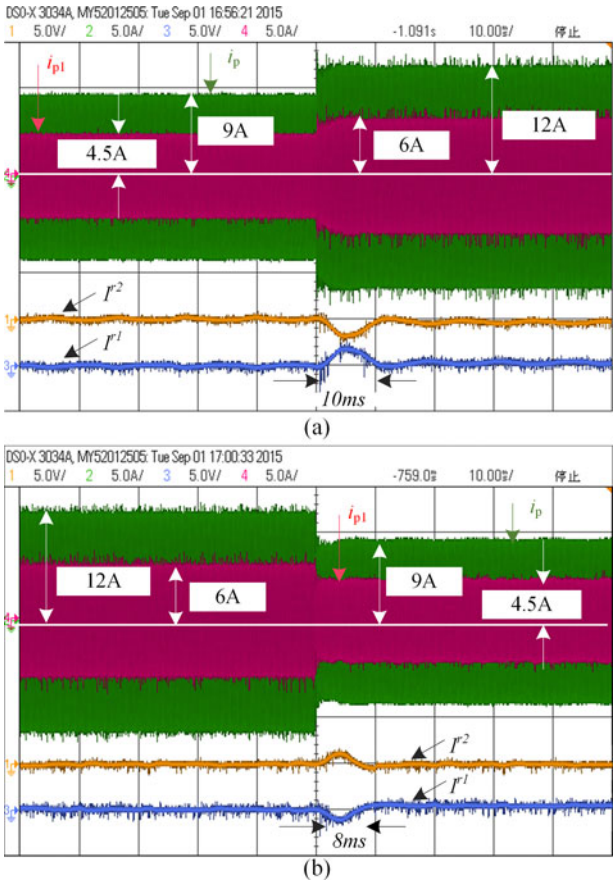

Fig. 19. Closed-loop system response to (a) step change in reference track current from 9 to 12 A, and (b) step change in reference track current from 12 to 9 A with asymmetrical inductance parameters.

1) Inverter Units With Asymmetrical Resonant Components: In a practical IPT system, it is unlikely for the resonant inverters to be identical. The tolerance for high-quality commercial inductors is about 10%.

As listed in Table I, the two inverter units have 10% difference in the resonant inductors ($L_2 = 0.9L_1$). The two inverter units are with the same dc input voltage ($E_1 = E_2 = 120$ V). The steady-state current waveforms without current sharing control [the same δ and θ as shown in (5)] are shown in Fig. 15. The track current is not evenly distributed in the two inverter units, and both amplitudes and phase angles of inverter units' output currents are different, due to the differences in the resonant inductors. The bottom waveform in Fig. 15 is the current

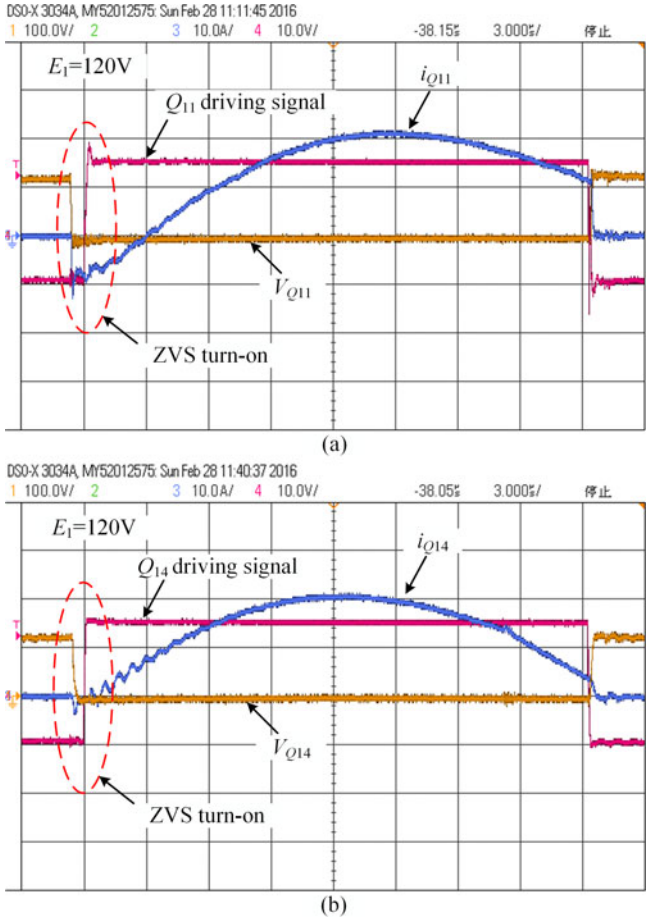

Fig. 20. Waveforms of MOSFETs (a) Q_{11} and (b) Q_{14} with current sharing control under asymmetrical inductance parameters condition.

difference between the two inverter units, which is twice of the circulating current. The amplitude values of the circulating current and track current are 1 and 15 A, respectively. It is evident that a large circulating current flows between the two inverter units under asymmetrical inductance parameters condition.

In Fig. 16, the current sharing control is applied to the IPT system based on two inverter units. The amplitude of track current is controlled to be 15 A. The track current is evenly distributed in the two inverter units, and the amplitude of circulating current is minimized to 0.125 A. The circulating current-associated power loss is very small that is valuable for industry applications. Fig. 17 shows the dc sources' output power and load power from power analyzer (YOKOGAWA WT1800). P_4, P_5, and P_6 are the input powers of two inverter units and the output power of the electronic load. The efficiency from dc power supplies to the electronic load can be calculated as $\eta = P_6/(P_4 + P_5) = \frac{2.8671}{1.5323+1.5327} \approx 93.54$ %. The system's power loss is about 198 W, and the measured power loss distribution is shown in Fig. 18. Furthermore, the output powers of the dc sources are identical that shows good power sharing can be achieved in a steady state with current sharing control.

The dynamic performances of track current under step change in the reference from 9 to 12 A are shown in Fig. 19(a). The proposed control method has a fast dynamic response

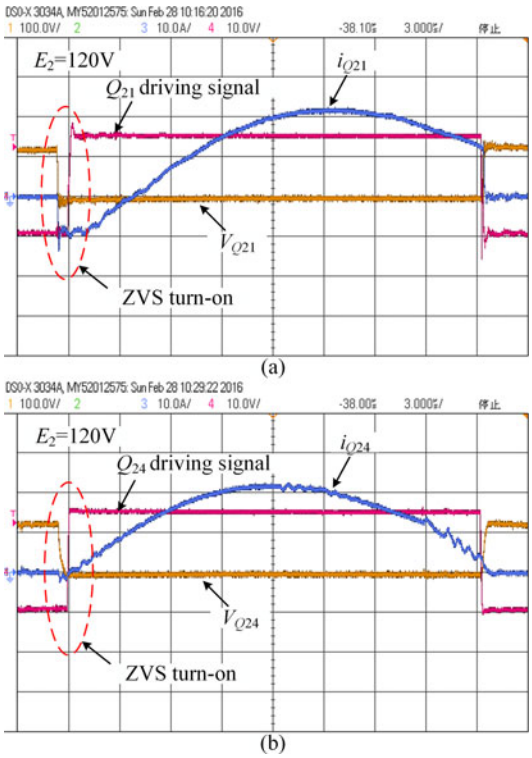

Fig. 21. Waveforms of MOSFETs (a) Q_{21} and (b) Q_{24} with current sharing control under asymmetrical inductance parameters condition.

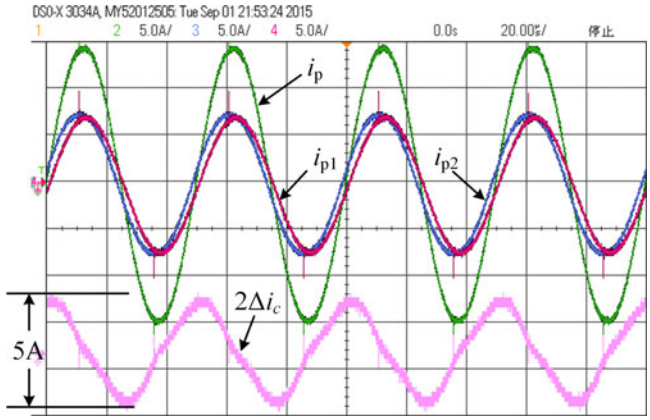

Fig. 22. Current waveforms without current sharing control under different dc sources condition.

performance with a settling time of 10 ms. The bottom waveforms in Fig. 19(a) are the reactive currents calculated by the controller and displayed by digital to analog converter, indicating that the reactive current control loop has a good dynamic performance. The dynamic performances of track current under step change in the reference from 12 to 9 A are shown in Fig. 19(b). The proposed control method has a fast dynamic response performance with a settling time of 8 ms.

The waveforms of MOSFETs in two inverters and corresponding driving signals under asymmetrical inductance parameters condition are depicted in Figs. 20 and 21. It should be noted that the two inverters can achieve ZVS turn-on operation with current sharing control.

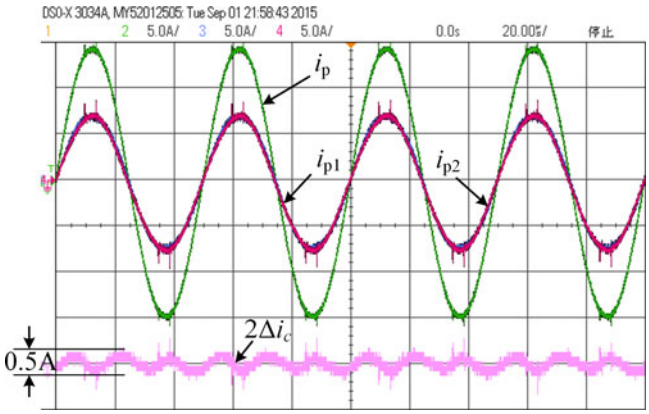

Fig. 23. Current waveforms with current sharing control under different dc sources condition.

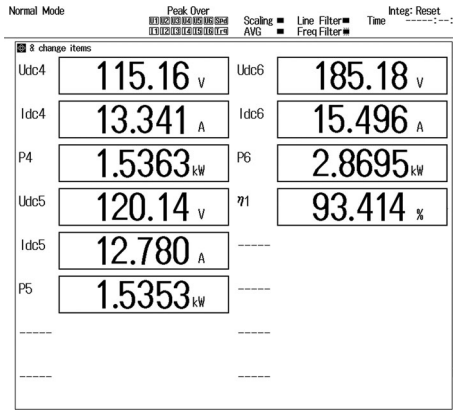

Fig. 24. Capture of power from power analyzer at 2.87 kW output with current sharing control under different dc sources condition.

2) Inverter Units With Different DC Sources: As discussed above, the inverter units feeding IPT systems can get power from different energy sources, e.g., the dc bus, batteries, and PV. In this case, it is necessary and important to investigate the performance of the system with different input dc voltages.

Not only there is 10% difference in the resonant inductors ($L_2 = 0.9L_1$), but also the input dc voltages are different ($E_1 = 115$ V and $E_2 = 120$ V). The steady-state current waveforms of the IPT system based on two inverter units without current sharing control are shown in Fig. 22. The amplitudes of the circulating current and track current are 1.25 and 15 A, respectively.

The circulating current can be controlled to be 0.125 A by employing the current sharing control as shown in Fig. 23. The track current is evenly distributed in the two inverter units as the last case does. In this case, both input power of each inverter unit are identical as shown in Fig. 24, which means good power sharing can be achieved in steady state with current sharing control with asymmetrical resonant components and different dc input voltages. The total efficiency from dc power supplies to the electronic load is up to 93.41%.

The dynamic performances of track current under step change in the reference from 9 to 12 A is shown in Fig. 25(a). The

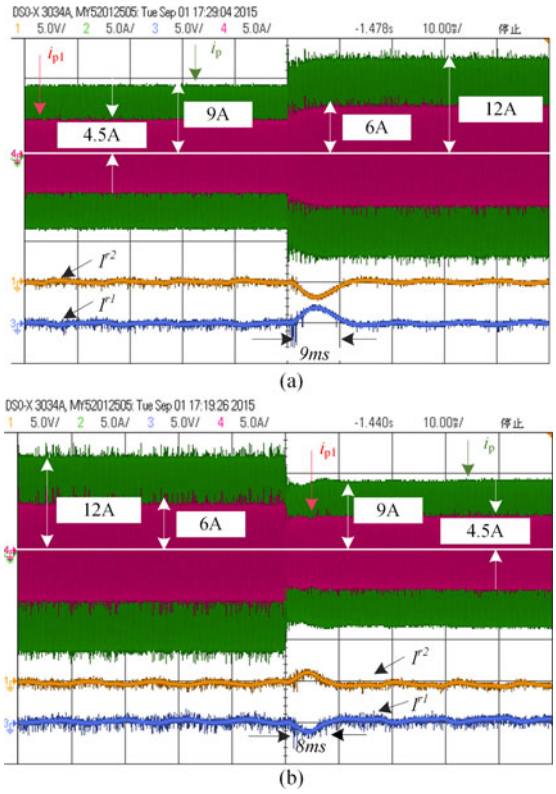

Fig. 25. Closed-loop system response to: (a) step change in reference track current from 9 to 12 A; and (b) step change in reference track current from 12 to 9 A under different dc sources condition.

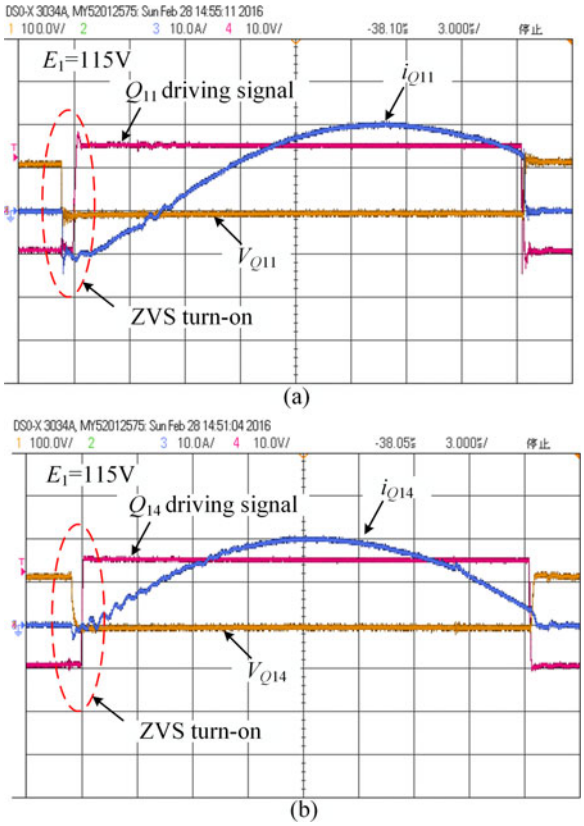

Fig. 26. Waveforms of MOSFETs (a) Q_{11} and (b) Q_{14} with current sharing control under different dc sources condition.

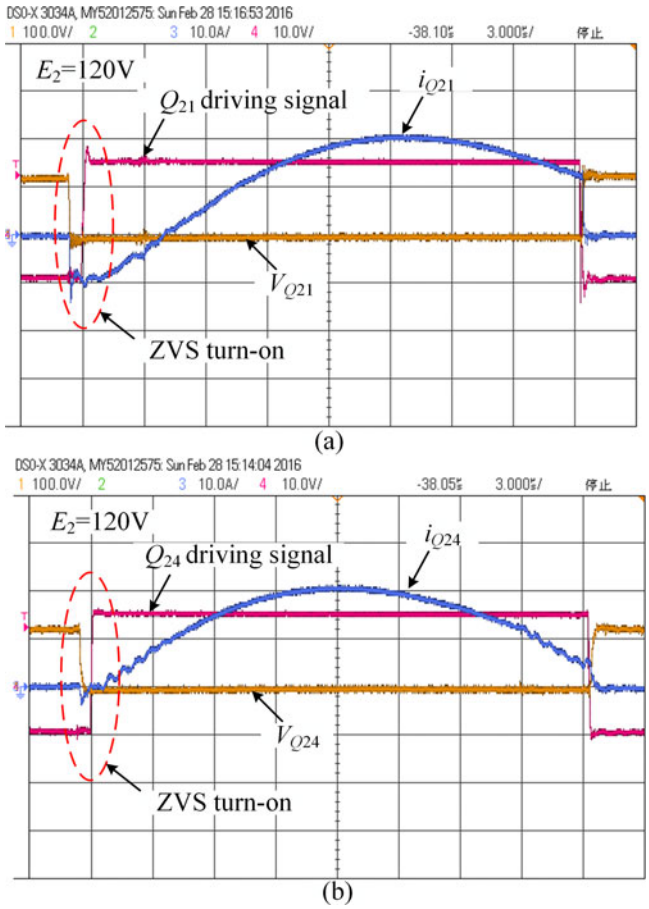

Fig. 27. Waveforms of MOSFETs (a) Q_{21} and (b) Q_{24} with current sharing control under different dc sources condition.

dynamic performances of track current under step change in the reference from 12 to 9 A are shown in Fig. 25(b). It can be shown that the proposed control method has good dynamic response performance with asymmetrical resonant components and different dc input voltages.

It is evident that the circulating current can be minimized and track current can be maintained to be constant with fast response by the proposed control method under steady state and transient states.

The waveforms of MOSFETs in two inverters and corresponding driving signals under different dc sources condition are demonstrated in Figs. 26 and 27. Similarly, all inverters can achieve ZVS turn-on operation with current sharing control.

3) Redundancy: For a practical multiinverter-based IPT system, it is desirable and necessary to investigate the performance of the system with faulty units. It can be seen from Fig. 28 that the amplitude of the track current control is to be 12 A in normal condition. Inverter unit 1 occurs a fault, and then is disconnected by the protection device. Finally, the input power stops flowing through the inverter unit 1. At the same time, the track current can be maintained to be 12 A by increasing the output current of inverter unit 2, although the inverter unit 1 current decreases to zero, which dramatically improving the availability and

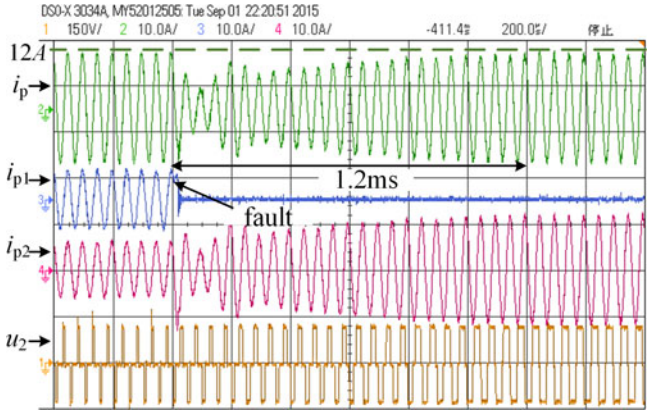

Fig. 28. Transient waveforms of the experimental system. The fault inverter unit 1 is disconnected and full compensation of the track current.

reliability. The system efficiency decreases to 85% because the primary circuit is not resonant after disconnecting the fault inverter unit, and the output current of available single inverter increases in order to maintain the track as a constant. The output voltage of the inverter shares quite a big phase difference with the current so the power loss of the inverter increases. The respond performance of the track current is 1.2 ms because there is only inverter unit 2 supplying the IPT system after disconnecting inverter unit 1. Therefore, only the active current controllers are operating.

V. Conclusion

A parallel multiinverter IPT system is presented in this paper to upgrade the power level of the IPT system. The operating principle of the proposed system and the influence factors of the circulating current have been analyzed and described in detail. Virtual active and reactive powers theory has been defined to decompose the active and reactive currents without PLL. Meanwhile, the active and reactive currents can be controlled independently to maintain a constant track current and minimize circulating currents. The availability and reliability of the proposed IPT system can be dramatically improved by the protection device. A 3-kW experimental prototype is set up and tested. The experimental results verify the performance of the proposed control approach.

The proposed method can upgrade the power level with low-cost semiconductor devices. Circulating current problem of the proposed IPT system is deliberately overcome by an active and reactive power decomposition without PLL. Not only more power can be transferred but also the circulating currents of two inverter units can be suppressed dynamically by the proposed method.

The proposed active and reactive currents decomposition-based control method is fully demonstrated by the 3-kW experimental prototype assembled in the university's lab. The high power level can be achieved employing the proposed method by adopting more inverter units connected in parallel and/or higher power level semiconductor devices and Litz wire, especially with the manufactured by industry companies.

References

[1] J. T. Boys, G. A. Covic, and A. W. Green, "Stability and control of inductively coupled power transfer systems," *Proc. IEE Electr. Power Appl.*, vol. 147, no. 1, pp. 37–43, Jan. 2000.

[2] D. J. Graham, J. A. Neasham, and B. S. Sharif, "Investigation of methods for data communication and power delivery through metals," *IEEE Trans. Ind. Electron.*, vol. 58, no. 10, pp. 4972–4980, Oct. 2011.

[3] M. R. Amini and H. Farzanehfard, "Three-phase soft-switching inverter with minimum components," *IEEE Trans. Ind. Electron.*, vol. 58, no. 6, pp. 2258–2264, Jun. 2011.

[4] Y. L. Li, Y. Sun, and X. Dai, "μ-Synthesis for frequency uncertainty of the ICPT system." *IEEE Trans. Ind. Electron.*, vol. 60, no. 1, pp. 291–300, Jan. 2013.

[5] J. G. Bum and B. H. Cho, "An energy transmission system for an artificial heart using leakage inductance compensation of transcutaneous transformer," *IEEE Trans. Power Electron.*, vol. 13, no. 6, pp. 1013–1022, Nov. 1998.

[6] S. Ping, A. P. Hu, S. Malpas, and D. Budgettt, "A frequency control method for regulating wireless power to implantable devices," *IEEE Trans. Biomed. Circuits Syst.*, vol. 2, no. 1, pp. 22–29, Mar. 2008.

[7] K. W. Klontz, D. M. Divan, D. W. Novotny, and R. D. Lorenz, "Contactless power delivery system for mining applications," *IEEE Trans. Ind. Appl.*, vol. 31, no. 1, pp. 27–35, Jan./Feb. 1995.

[8] J. Kuipers, H. Bruning, S. Bakker, and H. Rijnaarts, "Near field resonant inductive coupling to power electronic devices dispersed in water," *Sens. Actuators A, Phys.*, vol. 178, pp. 217–222, May 2012.

[9] S. Hasanzadeh, S. Vaez-Zadeh, and A.H. Isfahani, "Optimization of a contactless power transfer system for electric vehicles," *IEEE Trans. Veh. Technol.*, vol. 61, no. 8, pp. 3566–3573, Oct. 2012.

[10] K. D. Papastergiou and D. E. Macpherson, "An airborne radar power supply with contactless transfer of energy—Part-II: Converter design," *IEEE Trans. Ind. Electron.*, vol. 54, no. 5, pp. 2885–2893, Oct. 2007.

[11] N. A. Keeling, G. A. Covic, and J. T. Boys, "A unity-power-factor IPT Pickup for high-power applications," *IEEE Trans. Ind. Electron.*, vol. 57, no. 2, pp. 744–751, Feb. 2010.

[12] J. Shin, S. Shin, Y. Kim, S. Ahn, S. Lee, G. Jung, S. J. Jeon, and D. H. Cho, "Design and implementation of shaped magnetic resonance based wireless power transfer system for roadway-powered moving electric vehicles," *IEEE Trans. Ind. Electron.*, vol. 61, no. 3, pp. 1179–1192, Mar. 2014.

[13] U. K. Madawala and D. J. Thrimawithana, "A bidirectional inductive power interface for electric vehicles in V2G systems," *IEEE Trans. Ind. Electron.*, vol. 58, no. 10, pp. 4789–4796, Oct. 2011.

[14] G. A. J. Elliot, S. Raabe, G. A. Covic, and J. T. Boys, "Multiphase pick-ups for large lateral tolerance contactless power-transfer systems," *IEEE Trans. Ind. Electron.*, vol. 57, no. 5, pp. 1590–1598, May 2010.

[15] J. Huh, S. W. Lee, W. Y. Lee, G. H. Cho, and C. T. Rim, "Narrow-width inductive power transfer system for online electrical vehicles," *IEEE Trans. Power Electron.*, vol. 26, no. 12, pp. 3666–3679, Dec. 2011.

[16] S. Boyune, S. Jaegue, L. Seokhwan, S. Seungyong, K. Yangsu, J. Sungjeub, and J. Guho, "Design of a high power transfer pickup for on-line electric vehicle (OLEV)," in *Proc. IEEE Int. Electr. Veh. Conf.*, Mar. 2012, pp. 1–4.

[17] S. Chopra and P. Bauer, "Driving range extension of EV with on-road contactless power transfer—A case study," *IEEE Trans. Ind. Electron.*, vol. 60, no. 1, pp. 329–338, Jan. 2013.

[18] J. Kim, B. Lee, J. Lee, S. Lee, C. Park, S. Jung, S. Lee, K. Yi, and J. Baek, "Development of 1MW inductive power transfer system for a high speed train," *IEEE Trans. Ind. Electron.*, vol. 62, no. 10, pp. 6242–6250, Oct. 2015.

[19] A. P. Hu, "Selected resonant converters for IPT power supplies," Ph.D. dissertation, Dept. Electr. Electronic Eng., Univ. Auckland, Auckland, New Zealand, 2001.

[20] H. Hao, G. Covic, and J. T. Boys, "An approximate dynamic model of LCL-Based inductive power transfer power supplies," *IEEE Trans. Power Electron.*, vol. 29, no. 10, pp. 5554–5567, Oct. 2014.

[21] H. R. Rahnamae, D. J. Thrimawithana, and U. K. Madawala, "MOSFET based Multilevel converter for IPT systems," in *Proc. IEEE Int. Conf. Ind. Technol.*, Feb. 2014, pp. 295–300.

[22] H. R. Rahnamaee, U. K. Madawala, and D. J. Thrimawithana, "A multi-level converter for high power-high frequency IPT systems," in *Proc. IEEE 5th Int. Symp. Power Electron. Distrib. Gener. Syst.*, Jun. 2014, pp. 1–6.

[23] B. X. Nguyen, D. M. Vilathgamuwa, G. Foo, A. Ong, P. K. Sampathand, and U. K. Madawala, "Cascaded multilevel converter based bidirectional inductive power transfer (BIPT) system," in *Proc. ECCE-ASIA Int. Power Electron. Conf.*, May 2014, pp. 2722–2728.

[24] A. Schonknecht and R. W. A. A. De Doncker, "Novel topology for parallel connection of soft-switching high-power high-frequency inverters," *IEEE Trans. Ind. Appl.*, vol. 39, no. 2, pp. 550–555, Sep. 2003.
[25] H. Hao, G. A. Covic, and J. T. Boys, "A parallel topology for inductive power transfer power supplies," *IEEE Trans. Power Electron.*, vol. 29, no. 3, pp. 1140–1151, Mar. 2014.
[26] Z. Ye, P. K. Jain, and P. C. Sen, "Circulating current minimization in high-frequency AC power distribution architecture with multiple inverter modules operated in parallel," *IEEE Trans. Ind. Electron.*, vol. 54, no. 5, pp. 2673–2687, Oct. 2007.
[27] S. G. Xu, J. P. Xu, and J. P. Wng, "A current decoupling parallel control strategy of single phase inverter with voltage and current dual closed-loop feedback," *IEEE Trans. Ind. Electron.*, vol. 60, no. 4, pp. 1306–1313, Apr. 2013.
[28] B. X. Nguyen, D. M. Vilathgamuwa, G. H. B. Foo, P. Wang, A. Ong, U. K. Madawala, and T. D. Nguyen, "An efficiency optimization scheme for bidirectional inductive power transfer systems," *IEEE Trans. Power Electron.*, vol. 30, no. 11, pp. 6310–6319, Nov. 2015.
[29] U. K. Madawala, M. Neath, and D. J. Thrimawithana, "A power–frequency controller for bidirectional inductive power transfer systems," *IEEE Trans. Ind. Electron.*, vol. 60, no. 1, pp. 310–317, Jan. 2013.
[30] A. K. Swain, M. J. Neath, U. K. Madawala, and D. J. Thrimawithana, "A dynamic multivariable state-space model for bidirectional inductive power transfer systems," *IEEE Trans. Power Electron.*, vol. 27, no. 11, pp. 4772–4780, Nov. 2012.
[31] A. Okuno, H. Kawano, J. Sun, M. Kurokawa, A. Kojina, and M. Nakaoka, "Feasible development of soft-switched SIT inverter with load-adaptive frequency-tracking control scheme for induction heating," *IEEE Trans. Ind. Appl.*, vol. 34, no. 4, pp. 713–718, Jul. 1998.
[32] Y. Zhang, K. Chen, F. He, Z. Zhao, T. Lu, and L. Yuan, "Closed-Form oriented modeling and analysis of wireless power transfer system with constant-voltage source and load," *IEEE Trans. Power Electron.*, vol. 31, no. 5, pp. 3472–3481, May 2016.

Yong Li (S'15) received the B.Sc. degree in electrical engineering from Southwest Jiaotong University, Chengdu, China, in 2013, where he is currently working toward the Ph.D. degree in electrical engineering.

His main research interests include wireless power transfer and resonant converters.

Ruikun Mai (M'14) received the B.Sc. and Ph.D. degrees in electrical engineering from Southwest Jiaotong University, Chengdu, China, in 2004 and 2010, respectively.

He is currently an Associate Professor at the College of Electrical Engineering, Southwest Jiaotong University. His research interests include wireless power transfer and its application in railway systems, power system stability, and control.

Liwen Lu received the B.Sc. degree in electrical engineering from Southwest Jiaotong University, Chengdu, China, in 2014, where he is currently working toward the M.Sc. degree in electrical engineering.

His main research interest includes wireless power transfer.

Zhengyou He (M'10–SM'13) received the B.Sc. and M.Sc. degrees in computational mechanics from Chongqing University, Chongqing, China, in 1992 and 1995, respectively, and the Ph.D. degree in electrical engineering from Southwest Jiaotong University, Chengdu, China, in 2001.

He is currently a Professor at the College of Electrical Engineering, Southwest Jiaotong University. His research interests include signal process and information theory applied to electrical power system, and application of wavelet transforms in power system.